Complement C3 mediates early hippocampal neurodegeneration and memory impairment in experimental multiple sclerosis

Julien Bourel [a], Vincent Planche [b], Nadège Dubourdieu [a], Aymeric Oliveira [a], Alexandra Séré [c], Eva-Gunnel Ducourneau [a], Marion Tible [a], Marlène Maitre [a], Thierry Lesté-Lasserre [a], Agnes Nadjar [a,c], Aline Desmedt [a], Philippe Ciofi [a], Stéphane H. Oliet [a], Aude Panatier [a], Thomas Tourdias [a,d,*]

[a] Univ. Bordeaux, INSERM, Neurocentre Magendie, U1215, F-3300 Bordeaux, France
[b] Univ. Bordeaux, CNRS, UMR 5293, Institut des Maladies Neurodégénératives, F-33000 Bordeaux, France
[c] Univ. Bordeaux, INRAE, Bordeaux INP, NutriNeuro, UMR 1286, F-33000 Bordeaux, France
[d] CHU de Bordeaux, Neuroimagerie diagnostique et thérapeutique, F-33000 Bordeaux, France

ARTICLE INFO

ABSTRACT

Memory impairment is one of the disabling manifestations of multiple sclerosis (MS) possibly present from the early stages of the disease and for which there is no specific treatment. Hippocampal synaptic dysfunction and dendritic loss, associated with microglial activation, can underlie memory deficits, yet the molecular mechanisms driving such hippocampal neurodegeneration need to be elucidated. In early-stage experimental autoimmune encephalomyelitis (EAE) female mice, we assessed the expression level of molecules involved in microglia-neuron interactions within the dentate gyrus and found overexpression of genes of the complement pathway. Compared to sham immunized mice, the central element of the complement cascade, C3, showed the strongest and 10-fold upregulation, while there was no increase of downstream factors such as the terminal component C5. The combination of *in situ* hybridization with immunofluorescence showed that C3 transcripts were essentially produced by activated microglia. Pharmacological inhibition of C3 activity, by daily administration of rosmarinic acid, was sufficient to prevent early dendritic loss, microglia-mediated phagocytosis of synapses in the dentate gyrus, and memory impairment in EAE mice, while morphological markers of microglial activation were still observed. In line, when EAE was induced in C3 deficient mice (C3KO), dendrites and spines of the dentate gyrus as well as memory abilities were preserved. Altogether, these data highlight the central role of microglial C3 in early hippocampal neurodegeneration and memory impairment in EAE and, therefore, pave the way toward new neuroprotective strategies in MS to prevent cognitive deficit using complement inhibitors.

1. Introduction

Multiple sclerosis (MS) is the most frequent inflammatory disorder of the central nervous system (Compston and Coles, 2008). Impairment of episodic memory is one of the disabling manifestations that can occur early in the course of MS (Feuillet et al., 2007) with major impacts on the quality of life and the employment opportunities (Morrow et al., 2010). Memory impairment in MS patients has been correlated with hippocampal alterations as measured by magnetic resonance imaging (Sicotte et al., 2008), even after a single clinical event (Planche et al., 2017c). Based on this, the underlying cellular and molecular alterations within

the hippocampus are of great interest during early stage of MS, as their components could be used as targets in emerging therapeutic strategies.

Along these lines, experimental autoimmune encephalomyelitis (EAE) and pathological studies on post-mortem brains from patients have provided interesting cues (Di Filippo et al., 2018). In EAE, memory impairment was associated with alterations in hippocampal glutamatergic synaptic transmission (Habbas et al., 2015; Ziehn et al., 2012; Di Filippo et al., 2016; Di Filippo et al., 2013; Planche et al., 2017a) and with early synaptic and dendritic loss (Planche et al., 2017a; Ziehn et al., 2012; Ziehn et al., 2010). The number of dendritic spines was also found to be markedly reduced in *post-mortem* tissue from patients (Dutta et al.,

2011). This hippocampal synaptopathy (Mandolesi et al., 2015) was found to be secondary to pronounced activation of microglial cells (Ziehn et al., 2010; Ziehn et al., 2012; Di Filippo et al., 2013; Di Filippo et al., 2016; Planche et al., 2017a) which pin-point to the microglia-neuron communication as a possible key player in the cascade leading to early memory impairment.

Microglia can recognize and eventually phagocyte neuronal elements through different pathways involving distinct phagocytic receptors and opsonins depending on the conditions (Brown and Neher, 2014). Some components of the complement system are of particular interest in this cross-talk and have been well studied throughout brain development during which microglia can engulf unnecessary synapses and circuits tagged by complement proteins for elimination (Stevens et al., 2007; Schafer et al., 2012). Strikingly, this neurodevelopmental pathway could be aberrantly reactivated in neurodegenerative disorders such as Alzheimer's disease (Wu et al., 2019; Hong et al., 2016; Hansen et al., 2018; Shi et al., 2017) or glaucoma (Stevens et al., 2007; Howell et al., 2011) and participate to the progression of synaptic and dendritic loss.

Complement being part of the immune system, it is also activated in an auto-immune disease such as MS (Ricklin and Lambris, 2013). Specifically, activation of the complement is well described within inflammatory white matter lesions and can trigger the terminal assembly of C5b-C9 (membrane-attack-complex) leading to demyelination (Ingram et al., 2014). However, in the grey matter such as in the hippocampus, only limited inflammation has been reported in MS (Rocca et al., 2018) and the role of the complement in grey matter is still debated (Brink et al., 2005). Recently, partial activation without C5b-C9 deposits has been described within the hippocampus of post-mortem MS patients in association with dendritic loss and microglia activation (Michailidou et al., 2015) which is reminiscent of what was described in other neurodegenerative conditions (Stephan et al., 2012). However from this study on brain donors with long-lasting disease (Michailidou et al., 2015), it cannot be elucidated whether activation of the complement is a secondary mechanism to remove debris or whether it is a primary contributor to dendritic loss. Furthermore, the potential activation of the complement cascade during the early stage of MS is still a matter of controversy (Michailidou et al., 2017). Experimental research to elucidate these specific mechanisms of grey matter degeneration in MS has begun only recently. Werneburg et al. (2020) elegantly showed that the complement was involved in primary synaptic loss mediated by activated microglia, within the lateral geniculate nucleus of three different MS animal models; the retinogeniculate system being a network in which complement was already known to play key roles in the early postnatal development (Schafer et al., 2012). Yet, extension of this finding to the hippocampus and its relevance in terms of memory impairment had to be demonstrated. While Hammond et al. (2020) provided first cues in that sense, they explored the role of the complement in C3 knock out mice and this single condition cannot fully disentangle the possible role of C3 in active neurodegeneration from the role of C3 in the inflammatory cascade (Nataf et al., 2000; Szalai et al., 2007; Boos et al., 2004).

Therefore, the goal of this study was to investigate the complement system within the hippocampus at the early stage of experimental MS by combining pharmacological and knock out approaches. We provide evidence for microglial C3-mediated early dendritic loss within the dentate gyrus with causal role in early memory impairment which paves the way toward future therapeutic methods targeting this pathway.

2. Methods

2.1. Animals and induction of EAE

Experiments were performed on 6-to-10 weeks old wild type (WT) C57BL6/j female mice (Janvier Labs) and on homozygous C3 knock-out (KO) mice backcrossed onto the C57BL6/j background (Pekna et al.,

1998) kindly provided by Dr. T. Freitag (University of Helsinki, Finland). Female mice were preferred because of the higher prevalence of MS in female patients (Compston and Coles, 2008). Animals were housed in standard cages with a 12-h light/dark cycle and free access to food and water. All the experiments involving animals were conducted in accordance with the European directive (2010/63/EU) and after approval by the local ethical committee (approval numbers 10902 and 13517).

Active EAE was induced with a subcutaneous injection of 150 μg of myelin oligodendrocyte glycoprotein peptide 35–55 (MOG35–55, Anaspec) emulsified in 150 μl of Complete Freund's Adjuvant (CFA, Difco) containing 6 mg/ml of desiccated *mycobacterium tuberculosis* (Difco, H37Ra). Animals received intraperitoneal (i.p.) injections of pertussis toxin (Sigma) on the day of immunization and 2 days later (250 ng/injection). Control mice were injected with 150 μl of CFA emulsified in phosphate-buffered saline (PBS). All animals were weighted daily and scored for clinical symptoms using the standard grading scale (Baxter, 2007): 0, unaffected; 1: flaccid tail; 2: hind limb weakness and/or ataxia; 3: hind limb paralysis; 4: paralysis of all four limbs and 5: moribund.

The first clinical symptoms typically occur around 7-to-10 days post-immunization (dpi) in this model (Baxter, 2007). All the experiments reported in this article were conducted at 20 dpi, in line with our previous investigations (Planche et al., 2017a; Crombe et al., 2018), in order to investigate modifications that are specific to the early stage of MS (myelin antigen-induced immune activation) and not solely to peripheral inflammation (Konsman et al., 2002).

2.2. Drugs

In dedicated experiments (between 5 and 18 animals depending on experiments), pharmacological inhibition of C3 was performed using rosmarinic acid (RMA). RMA can pass the blood brain barrier and was found to inhibit complement activation predominately by blocking C3b attachment to complement-activating surfaces (Sahu et al., 1999). RMA was dissolved in sterile isotonic 0.5% PBS-DMSO solution and used at 2.5 mg/kg concentration. Mice treated with RMA received daily i.p. injections of 250 μl of RMA solution from 7 dpi to 20 dpi. We chose to start the treatment at 7dpi because it is the typical beginning of first behavioral symptoms in EAE mice (Acharjee et al., 2013; Haji et al., 2012). The control groups received daily i.p. injections of 250 μl of 0.5% PBS-DMSO and were referred as vehicle (Veh) groups.

2.3. Laser capture microdissection (LCM) and quantitative real-time PCR (qPCR) analyses

We (Planche et al., 2017a; Crombe et al., 2018) and others (Habbas et al., 2015) have previously found that the dentate gyrus was particularly vulnerable at the early stage of EAE and was characterized by dendritic and electrophysiological alterations of the granule neurons projecting within the adjacent molecular layer, this being accompanied by microglia activation. Therefore, we microdissected the molecular layer of the dentate gyrus to screen for modifications of expression of genes involved in the neuron-to-microglia interactions (Brown and Neher, 2014).

At 20 dpi, mice were sacrificed ($N = 10$ EAE and N = 10 CFA) and their brains were quickly extracted, flash-frozen using isopentane cooled by dry ice and subsequently stored at -80 °C until sectioning. Frozen brains were thawed to -20 °C in a cryostat chamber (CM3050-S, Leica Microsystems) and coronally sectioned at 40 μm. Slices collected from bregma -1 mm to -2.54 mm were mounted on polyethylene-naphthalate membrane 1 mm glass slides (P.A.L.M. Microlaser Technologies AG) pre-treated to inactivate RNase. The sections were immediately fixed with 95% ethanol, followed by 75% and 50% ethanol (30 s each). Sections were stained with 1% cresyl violet in 50% ethanol for 30 s and dehydrated once in 50%, 75% and 95% and twice in 100% ethanol

(30 s each). Laser Pressure Catapulting microdissection (LPC) of samples was performed using a PALM MicroBeam microdissection system version 4.6 equipped with the P.A.L.M. RoboSoftware (P.A.L.M. Microlaser Technologies AG). Laser power and duration were adjusted to optimize capture efficiency. Microdissection was performed at a 5× magnification and selectively excised the molecular layer of the dentate gyrus (see Fig. 1A). The microdissected samples were collected in adhesives caps and re-suspended in 250 μl guanidine isothiocyanate-containing buffer (ReliaPrep™ RNA Cell Miniprep System, Promega) with 10 μl 1-thioglycerol, and stored at −80 °C until extraction was done. Total RNA was extracted using the ReliaPrep™ RNA Cell Miniprep System (Promega) according to the manufacturer's protocol. The integrity of RNA was checked by capillary electrophoresis using the RNA 6000 Pico Labchip kit and the Bioanalyser 2100 (Agilent Technologies), and quantity was estimated using a Nanodrop 1000 (Thermo Scientific). The RNA integrity numbers (RIN) were always above 7/9.

RNA was processed and analyzed according to published guidelines (Bustin et al., 2009). Briefly, cDNA was synthesized from 84 ng of total RNA by using qSript™ cDNA SuperMix (Quanta Biosciences). The qPCR was performed with a LightCycler® 480 Real-Time PCR System (Roche). The qPCR reactions were run in duplicate for each sample by using LightCycler 480 SYBR Green I Master (Roche) in a final volume of 10 μl. The qPCR data were exported and analyzed in an informatics tool (Gene Expression Analysis Software Environment) developed by our core facility. The Genorm method was used to determine the reference gene (Bustin et al., 2009). Relative expression analysis was normalized against two reference genes. In particular, Glyceraldehyde-3-Phosphate Dehydrogenase (*Gapdh*) and Elongation factor 1-alpha 1 (*Eef1a1*) were used as reference genes here. The relative level of expression was calculated with the comparative ($2^{-\Delta\Delta CT}$) method (Livak and Schmittgen, 2001). Primer sequences are reported in **Supplemental Table 1**.

2.4. Quantification of C3 protein

At 20 dpi, mice were sacrificed (*N* = 8 EAE and N = 8 CFA) and their brains were quickly extracted, flash-frozen using isopentane cooled by dry ice and subsequently stored at −80 °C until sectioning. The molecular layer of the dentate gyrus was laser microdissected following the steps described above and samples were incubated for 10 min at room temperature in a lysis buffer (TBS 1×, Triton 0.1×, protease inhibitor). The samples were sonicated for 5 s and centrifuged at 11000 rpm for 1 h at 4 °C, and the supernatants collected. Protein quantification was performed using the Micron BCA™ protein assay reagent kit (Thermoscientific, 23,225). Then, C3 protein was quantified by enzyme-linked immunosorbent assay (ELISA). We used a kit with a 96-well plate pre-coated C3 according to the manufacturer's instructions (Genway Biotech Inc., GWB-7555C7). Briefly, samples were diluted 1:4, added to the wells and detection was carried out with an anti-C3 HRP-conjugated detector antibody with H_2O_2 and 3,3′-5,5′-tetramethylbenzidine as a chromogen. Each sample was run in duplicate and mean optical density (which is proportional to the amount of C3) was measured at 450 nm using a microplate absorbance reader. Amount of C3 was normalized to the total protein content.

2.5. In situ hybridization using RNAScope

To discriminate the cellular origin of C3, we used RNAScope to co-localize the fluorescent C3-mRNA hybridization signal with phenotypic markers of microglia (Iba1), astrocytes (GFAP) and neurons (NeuN).

RNAScope technology is an *in situ* hybridization approach sensitive enough to visualize single RNA molecules per cell and was used here following previously published method (Mishra et al., 2019). Briefly, mice (*N* = 12 EAE) were sacrificed at 20 dpi and their brains were quickly extracted and flash-frozen using isopentane cooled by dry ice and subsequently stored at −80 °C until use. Fourteen-μm thick sections

were cut in a cryostat, mounted on superfrost slides and fixed overnight in 10% formalin at 4 °C. Sections were dehydrated in 50%, 70% and 100% ethanol (5 min each), treated with hydrogen peroxide 10 min at room temperature, and incubated in a protease solution for 20 min at room temperature followed by a 15 min wash in PBS. Target probe specific for C3 (as well as a positive control probe targeting the housekeeping gene *Ppib* and a negative control probe targeting the bacterial gene *dapB*) were applied on series of neighboring sections and incubated for 2 h at 40 °C in a specific oven (HybEZ Hybridization System). Sections were next incubated with multi step preamplifier and amplifier probes (from AMP1 to AMP6) to amplify the signal that was finally detected with the fluorescent label fast RED-B (10 min at room temperature).

### 2.6. Combination of RNAScope with immunocytochemistry (ICC) and image analyses

Hybridized sections were randomly divided in 3 groups (*N* = 4/ group) and incubated overnight at room temperature with primary antisera to Iba1 (rabbit; 1:2000; Wako, 019–19,741), GFAP (rabbit; 1:1000; Dako, ZO334), or NeuN (chicken; 1:1000; Merck, ABN91). The day after, the following secondary antibodies were applied for 2 h at room temperature: HRP-anti-rabbit IgG for Iba1 (goat; 1:500; Cell Signaling, 7074S) followed by amplification with 1:2000 TSA-fluorescein (PerkinElmer, FP1135) for 10 min, Alexa 488-anti-rabbit IgG for GFAP (donkey; 1:2000; Jackson Immunoresearch, 711–545-152), and Alexa 488-anti-chicken IgG for NeuN (donkey; 1:2000; Jackson Immunoresearch, 703–545-155). Cell nuclei were stained with bis-Benzimide (60 s; diluted 1:10⁶; Hoechst No. 32258).

RNAScope-ICC dual fluorescent sections were observed on a SP8 confocal microscope (Leica). For analyses, images were captured with a 40× water immersion objective. At least 4 optical stacks (separate channels mode, z = 12 confocal frames, 1.0 μm-thick, acquired in 0.5 μm steps, and 276 × 276 μm in area) were acquired in the molecular layer of the dentate gyrus in two to four sections per animal. Image analysis using ImageJ software (imagej.nih.gov) consisted in counting profiles of C3 mRNA-positive cells and classifying them as positive or negative for either ICC cell marker (C3/Iba1+ or C3/Iba1-; C3/GFAP+ or C3/GFAP-; C3/NeuN+ or C3/NeuN-).

2.7. Golgi staining, neuromorphometric and dendritic spines analyses

The FD Rapid Golgi Stain kit (FD Neurotechnologies, INC), a simplified and reliable kit for Golgi impregnation, was used to visualize the morphology of the granule neurons of the dentate gyrus as described previously (Shi et al., 2015). Mice were sacrificed at 20 dpi (between 5 and 8 mice per group) and brains were immediately dissected out and rinsed in MilliQ water. Then, brains were immerged in a Golgi-cox solution comprising potassium dichromate, mercuric chloride and potassium chromate for 10 days. The brains were then transferred to a cryoprotectant solution and stored for 2 days at 4 °C prior to be frozen at −60 °C in isopentane. Then, 100 μm thick sections were cut in the coronal plane in a cryostat. Sections were mounted onto gelatin-coated slides and air dried at room temperature in the dark. After drying, sections were rinsed with distilled water, stained in the developing solution and dehydrated in baths of ethanol at increasing concentration followed by xylene substitution for defatting.

Morphometric analyses of the dendritic arbor of the granule neurons of the dentate gyrus were performed using a 40× objective of a Leica microscope coupled to a manual neuron tracing system (NeuroLucida, MicroBrigthField Bioscience). Between 3-to-5 neurons per animal (*n* = 25 to 29 neurons per group) were selected blind to the experimental condition and based on the following standard criteria: *(i)* the cell body should be contained in the slice, *(ii)* the dendrites should be vertically oriented within the molecular layer, and *(iii)* the overlap with the dendrites of the adjacent cells should be minimal, to avoid ambiguous
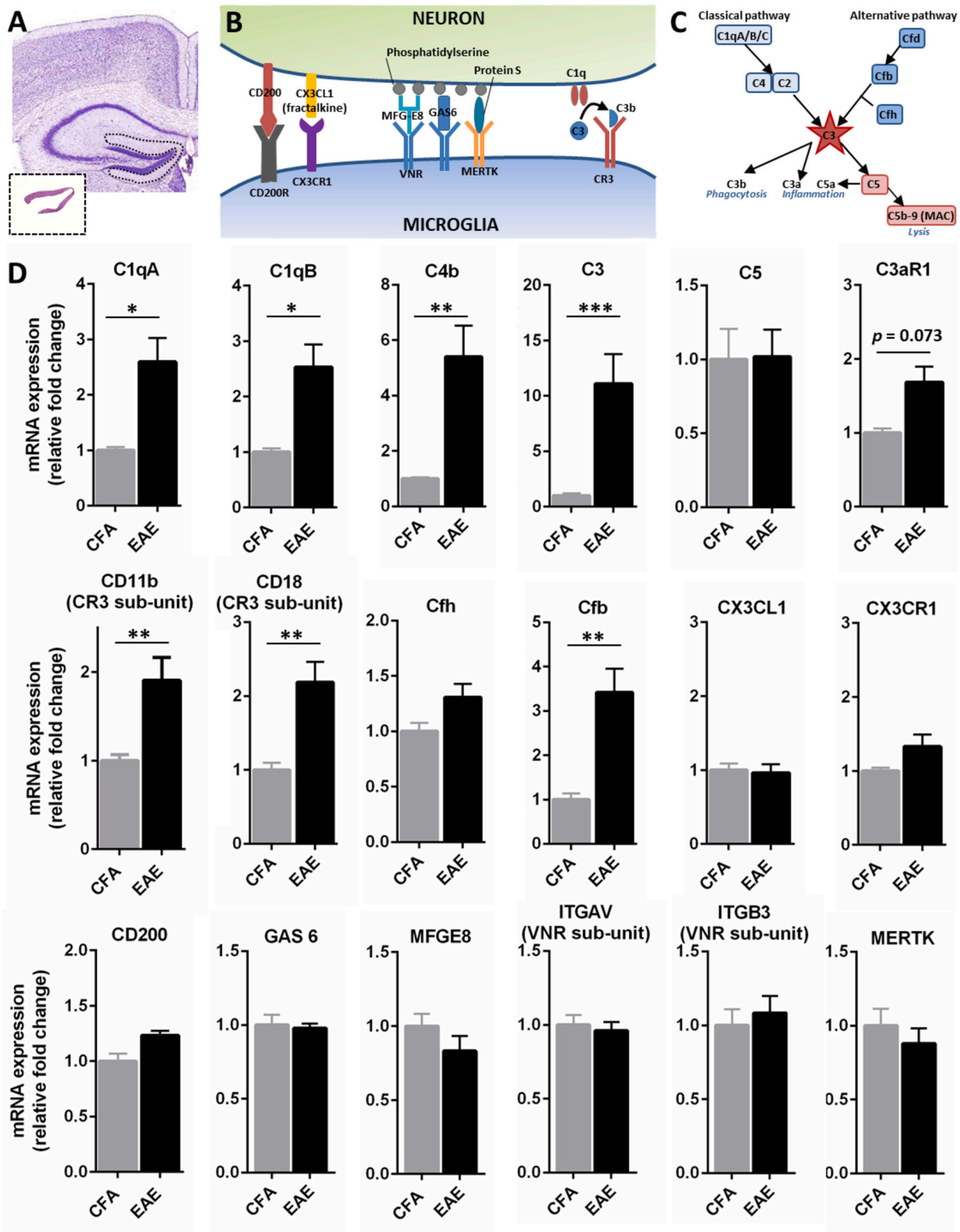
Fig. 1. Expression of genes involved in microglia-neuron interactions in the dentate gyrus of EAE- and control CFA-mice.
(**A**) Illustration of the laser-microdissected area (dotted line, molecular layer of the dentate gyrus) that was further used for gene expression quantification. (**B**) Schematic representation of the signaling pathways involved in microglia-to-neuron interactions (adapted from Brown et al., (2014)). (**C**) Simplified schematic representation of the complement pathway (adapted from Veerhuis et al., (2011)). (**D**) Relative expression of genes within the molecular layer of the dentate gyrus in EAE and CFA mice at 20 dpi.
Error bars indicate mean ± SEM. EAE: $N = 10$ mice and CFA: N = 10 mice. * $p < 0.05$, ** $p \leq 0.01$, *** $p \leq 0.001$ for unpaired Student's t-test or Mann-Whitney test according to normality distribution, and with Bonferroni correction (*i.e.* $n = 18$ comparisons). (For interpretation of the references to colour in this figure legend, the reader is referred to the web version of this article.)

tracing of the dendritic tree. For each neuron, the total dendritic length and the total number of nodes were analyzed.

For spine analyses, sections were observed with a DM5000 microscope (Leica Biosystems Company) at a $100\times$ magnification. Stacks of 15-to-50 frames (0.2 μm-thick) were acquired from at least 4 granule neurons per animal ($N = 4$ animals per groups) and 2-to-5 dendrites were analyzed per neuron for a total of 54-to-61 dendrites per group. Within distal segments long of 20-to-40 μm, the number of spines was counted automatically using ImageJ and Neuronstudio software.

2.8. Standard immunohistochemistry and image analyses

Mice ($N = 5$ per group) were deeply anesthetized at 20 dpi with exagon/lidocaïne and perfused transcardially with saline followed by a PBS solution containing 2% paraformaldehyde and 0.2% picric acid, for 20 min. The brains were then removed and transferred into a Tris-buffered saline (TBS) containing 30% sucrose and 0.05% sodium azide and stored at 4 °C until use. A tissue block containing the dorsal hippocampus was cut into 30 μm thick coronal sections in a cryostat.

2.8.1. Cell numbers and labeling distribution

Single immunostaining was performed for microglia (anti-Iba1), astrocytes (anti-GFAP), myelin basic protein (anti-MBP) and T lymphocytes (anti-CD3). Free-floating sections were rinsed in TBS and incubated overnight in a TBS solution containing 0.25% Triton X-100, 1% normal donkey serum and diluted primary antiserum. The following rabbit antisera were used: anti-Iba1 (1:2000; Wako, 19–19,741), anti-GFAP (1:1000; Dako, Z0334), anti-MBP (1:1000; Abcam, ab 40,390) and anti-CD3 (1:200, Abcam, ab 5690). Afterwards, sections were washed in TBS and incubated with Alexa Fluor 488-donkey anti-rabbit IgGs (1:1000; Jackson Laboratories, 711–545-152) in a TBS solution containing 0.25% Triton X100 (2 h at room temperature). A mounting medium containing DAPI was used for coverslipping (Vectashield H-1200).

Sections were imaged for quantitative analyses on a video-spinning-disk laser confocal microscope (Leica DMI 6000) equipped with a $20\times$ objective and with a camera Coolsnap HQ2 (Photometrics). These systems were driven by Metamorph software (Molecular Devices) and the "scan slide" mode was used in order to visualize and reconstruct mosaics of the whole dentate gyrus from 1 μm-thick confocal frames. Identical laser intensity and exposure settings were applied to all tissue sections. At least 2 tissue sections containing the dorsal hippocampus were randomly selected per group and quantitative results were averaged. Images were analyzed using ImageJ software. Regions of interest (ROI) outlining the molecular layer of the dentate gyrus were manually drawn on the mosaic and cell profiles were counted when exhibiting a DAPI-stained nucleus. Within the ROIs, microglial cells (Iba1+/DAPI+), astrocytes (GFAP+/DAPI+) and T lymphocytes (CD3+/DAPI+) were counted manually and their number normalized by the size of the ROI. Iba1, GFAP and MBP staining area were also quantified automatically as percent area of immunoreactivity (after subtracting background and thresholding identically all the images for conversion to binary masks).

2.8.2. Microglial phagocytosis

To analyze microglial engulfment of synapses we performed a triple immunostaining for microglia (Iba1), for the lysosomal marker CD68 and for the post-synaptic marker Homer 1,2,3. Free-floating sections were rinsed in TBS and incubated in 3% H_2O_2 for 30 min before overnight incubation with the primary antisera. The following primary antisera were used: anti-Iba1 (goat; 1:2000; Abcam, Ab5076), anti-CD68 (rat; 1:1000; AbD Serotec, MCA 1957) and anti-homer 1,2,3 (rabbit; 1:500; Synaptic System, 160,103) in a TBS solution containing 1% of normal donkey serum and 0.25% triton x100. After incubation, tissue

sections were washed in TBS and incubated with the following secondary antibodies in a PBS $1\times$ solution containing 0.25% Triton X100 for 2 h at room temperature: HRP-donkey anti-goat IgGs (1:500; Invitrogen, A16005) followed by amplification with TSA-cyanine 3 (1:2000; PerkinElmer, FP1135) for 10 min, Cyanine 5-donkey anti rat IgGs (1:1000; Jackson Immunoresearch, 712–175-150) and Alexa 488-donkey anti-rabbit IgGs (1:1000; Jackson Immunoresearch, 711–545-152). Cell nuclei were stained with bis-Benzimide (60 s; diluted 1:10^6; Hoechst No. 32258).

Sections were observed on a SP8 confocal microscope (Leica) and microglial engulfment analysis was performed with a protocol derived from previously published methodology (Dejanovic et al., 2018). Briefly, under a $63\times$ oil immersion objective, optical stacks (separate channel mode, z = 30-to-140 frames, 0.42 μm-thick, steps of 0.21 μm, and of 146×146 μm in area) were acquired in the molecular layer of the dentate gyrus in 2-to-3 tissue sections per animal ($N = 5$ animals per group) to reconstruct 3-to-8 microglia cells per section; counting included a total of 30-to-49 microglial cells per group. Microglial cells and their CD68-positive lysosomes were 3D-reconstructed using the surface rendering function in Imaris 9.2 and homer-positive puncta inside the lysosomes were quantified using the spot function all blind to the experimental conditions.

2.9. Contextual fear conditioning protocol

Memory was assessed with a contextual fear conditioning protocol. We showed previously that this hippocampus-dependent contextual learning (Kaouane et al., 2012; Calandreau et al., 2006) was impaired in EAE mice and was particularly suitable in the context of EAE as it doesn't require important motor skills (Planche et al., 2017a).

Briefly (see Fig. 6A for a schematic representation of the protocol), acquisition of fear conditioning in mice ($N = 13$ to 18 per group) took place in a brightness of 60 lx in a transparent plexiglas box giving access to different visual-spatial cues in the experimental room. The floor of the chamber consisted of stainless-steel rods connected to a shock generator. The box was cleaned with 70% ethanol. The training procedure consisted in a pseudo-random distribution of tones and shocks as follows (tone-shock unpairing procedure): 100 s after being placed into the chamber, animals received a footshock (0.4 mA squared signal, 1 s), then, after 20 s, a tone (65 dB, 1 kHz, 15 s) was presented twice (30 s delay); finally, after 30 s, mice received a second shock and returned to the home cage 20 s thereafter. As the tone is never followed by shock delivery, animals normally identify the conditioning context (set of static background contextual cues that constitutes the environment in which the conditioning takes place), and not the tone, as the right predictor of the shock. A relatively high fear response to the predictive context associated with no fear response to the tone are thus expected.

One day after the acquisition, mice were re-exposed to the tone alone during 2 min in a safe and familiar chamber where they had been pre-exposed the day before conditioning (opaque PVC chamber with opaque floor, brightness of 15 lx, cleaned with 4% acetic acid) and three successive recording sessions of behavioral responses were performed: one before (first 2 min), one during (next 2 min), and one after (2 last min) tone presentation. Two hours later, animals were re-exposed to the conditioning context alone, without the tone. Animals were recorded on videotape for off-line manual scoring of freezing behavior.

Conditioned fear to the context was assessed by measuring the percentage of total time spent freezing during 3 blocks of 2 min each (0–2, 2–4 and 4–6 min). Because the fear response naturally decreases over time, quantitative analyses were conducted only on the first 2 min period of context re-exposure as previously done (Kaouane et al., 2012; Planche et al., 2017a; Calandreau et al., 2006). In order to assess a possible abnormal fear memory for the (not predictive) salient tone, the

percentage of freezing during the tone presentation is measured, and the strength of this conditioned fear is attested by a ratio that considers the percentage of freezing increase to the tone with respect to a baseline freezing level (*i.e.*, pre- and post-tone periods mean):

$$\frac{\%\text{freezing during the tone} - (\%\text{pretone period freezing} + \%\text{posttone period freezing})/2}{\%\text{freezing during the tone} + (\%\text{pretone period freezing} + \%\text{posttone period freezing})/2}$$

Two different observers performed the measurements independently in a sub-sample of 12 experiments with good reproducibility (intra-class correlation coefficient = 0.89, $p < 0.05$).

2.10. Statistical analyses

All the investigations described above (neuromorphometric analyses, spine and microglial cell counting, engulfment assay, freezing measurements) were conducted blind to the experimental conditions. Data are presented as mean ± SEM. The Gaussian distribution was tested with Shapiro-Wilk normality test. Comparisons of clinical scores over time between groups were conducted by using a two-way ANOVA. Gene expressions were compared between EAE and CFA with unpaired *t*-tests or Mann-Whitney tests as appropriate. To reduce the risk of type I error due to the repetition of comparisons, the Bonferroni correction was used (correction for 18 comparisons). Proportions of C3+ and C3- in each cell type were compared with the chi^2 test. For the other comparisons that were conducted in more than 2 groups, we used a one-way ANOVA or Kruskal-Wallis test as appropriate followed by post-hoc comparisons using Tukey's multiple comparisons test or false discovery rate (FDR) correction. All the statistical analyses were performed with Prism 6.05 (GraphPad Software, La Jolla, CA, USA). **Supplemental Table 2** summarizes the number of animals and the statistical tests used for each experimental procedure.

3. Results

3.1. Microglia-mediated induction of complement expression within the dentate gyrus of EAE mice

We (Planche et al., 2017a) and others (Habbas et al., 2015) previously reported a spatial selectivity in the inflammation processes during the early stage of EAE, as it was predominant in hippocampal areas surrounding the third ventricle, especially the dentate gyrus. This led to the concept of differential vulnerability of the dentate gyrus (Planche et al., 2017a; Small, 2014) as a critical element for memory impairment in the early stage of EAE; an observation that is also likely to hold true in MS patients (Planche et al., 2018). Because we previously observed dendritic alterations associated with microglia activation in the dentate gyrus (Planche et al., 2017a; Crombe et al., 2018), we first screened the expression of genes involved in microglial phagocytic signaling with qPCR specifically within this brain region.

At 20 dpi, EAE ($N = 10$) and control mice receiving only Complete Freund's Adjuvant (CFA, N = 10) mice were sacrificed. The molecular layer of the dentate gyrus was laser-microdissected (Fig. 1A) to perform RTqPCR experiments after RNA extraction. Most common signaling pathways implicated in the phagocytosis of neuronal elements by microglia were screened (Fig. 1B) including the complement cascade (Fig. 1C). Our results showed that EAE altered the expression levels of genes from the classical complement pathway *i.e.* (C1qA, C1qB, C4b, C3 mRNA) and also genes involved in the alternative pathway such as Cfb mRNA (Fig. 1D). The expression level of Cfh mRNA, which is an inhibitory molecule of complement activation (Stephan et al., 2012),

was unchanged in EAE-mice. The major complement component C3, that is the point of convergence of the different pathways (Fig. 1C), showed the strongest upregulation, up to a ten-fold (mean relative fold change = $11.10 \pm 2.68$ *vs.* 1.00 ± 0.22 in EAE, N = 10, and CFA, N = 10, respectively, $p < 0.0001$, Mann-Whitney test, Fig. 1D). Importantly, we did not find any modification of C5 mRNA expression suggesting that the terminal lytic pathway was not involved. The microglia-specific receptor of C3b (*CD11b* and *CD18* sub-units) was also upregulated. Furthermore, none of the other tested genes displayed modification of their expression in EAE- compared to CFA-mice. While this screening was limited to only few important pathways, it suggested the primary involvement of the complement pathway in this pathological microglia-neuron interaction (Fig. 1D).

We next focused on C3, as this central element was the most up-regulated. We first confirmed with an ELISA test directed against the C3 protein, that it was strongly over-expressed in the dentate gyrus of EAE-mice compared to CFA-mice (mean C3 protein concentration = 124.8 ± 29.35 ng/mg *vs.* 49.3 ± 5.97 ng/mg in EAE, $N = 8$, and CFA, N = 8, respectively, $p = 0.0011$, Mann-Whitney test, Fig. 2A). As complement components can be locally produced by glial cells or by neurons with differential involvement of each cell types according to the conditions (Veerhuis et al., 2011), we determined which cell type was responsible for the most abundant synthesis of C3 in EAE-mice ($N = 12$) at 20 dpi. Pre-treatments of RNAscope were adjusted (see method) to ensure good RNA quality and fixation conditions leading to strong positive control probe staining and clean negative probe staining with no background (Fig. 2B and C). By combining such RNAscope method with immunofluorescence we observed that C3 transcripts were mainly produced by microglia/myeloid cells (mean co-localisation = $82.54 \pm 5.98\%$, $N = 4$ mice and $n = 4$ optical stacks per animal, Fig. 2D), with significantly lower residual C3 expression in astrocytes (mean co-localisation = $12.36 \pm 3.31\%$, N = 4 mice and n = 4 optical stacks per animal, $p < 0.0001$, chi^2 test, Fig. 2E) and neurons (mean co-localisation = $2.73 \pm 1.25\%$, N = 4 mice and n = 4 optical stacks per animal, $p < 0.0001$, chi^2 test, Fig. 2F). CD3 revealed the absence of T lymphocytes infiltration in the hippocampus as classically reported at this stage of EAE (t Hart et al., 2011) where plaques are predominantly found in the spinal cord (Planche et al., 2017a). Therefore, microglial cells were responsible for the bulk of C3 production in the dentate gyrus.

### 3.2. C3 inhibitor reduces dendritic loss in the dentate gyrus of EAE-mice

To assess the consequences of increased C3 on neurons, we performed morphometric analyses of the dendrites of dentate gyrus granule neurons in the molecular layer by using Golgi staining ($n = 25$ to 29 neurons per condition) both, in mice treated with RMA ($N = 5$ to 8), a blocker of downstream C3 activation (Sahu et al., 1999) and in untreated mice (Veh, N = 5 to 8).

We found a significant reduction in the total dendritic length and complexity of the granule neurons in EAE-mice compared to CFA-mice (919 ± 42.7 µm *vs.* 1085 ± 54.1 µm in length, $p < 0.05$ and 5.3 ± 0.28 nodes *vs.* 6.8 ± 0.39 nodes, in EAE-Veh and CFA-Veh respectively, $p < 0.05$, one-way ANOVA and Tukey *post hoc*, Fig. 3A and B). We also found a significant variation of spine density along the distal dendrites among groups ($n = 54$ to 61 dendrites per conditions from N = 4 mice per groups, F = 5.1, $p = 0.0022$, one-way ANOVA) with a reduction in EAE-mice compared to CFA-mice which was close to significance when using *post-hoc* analyses corrected for multiple comparisons (12.8 ± 0.55
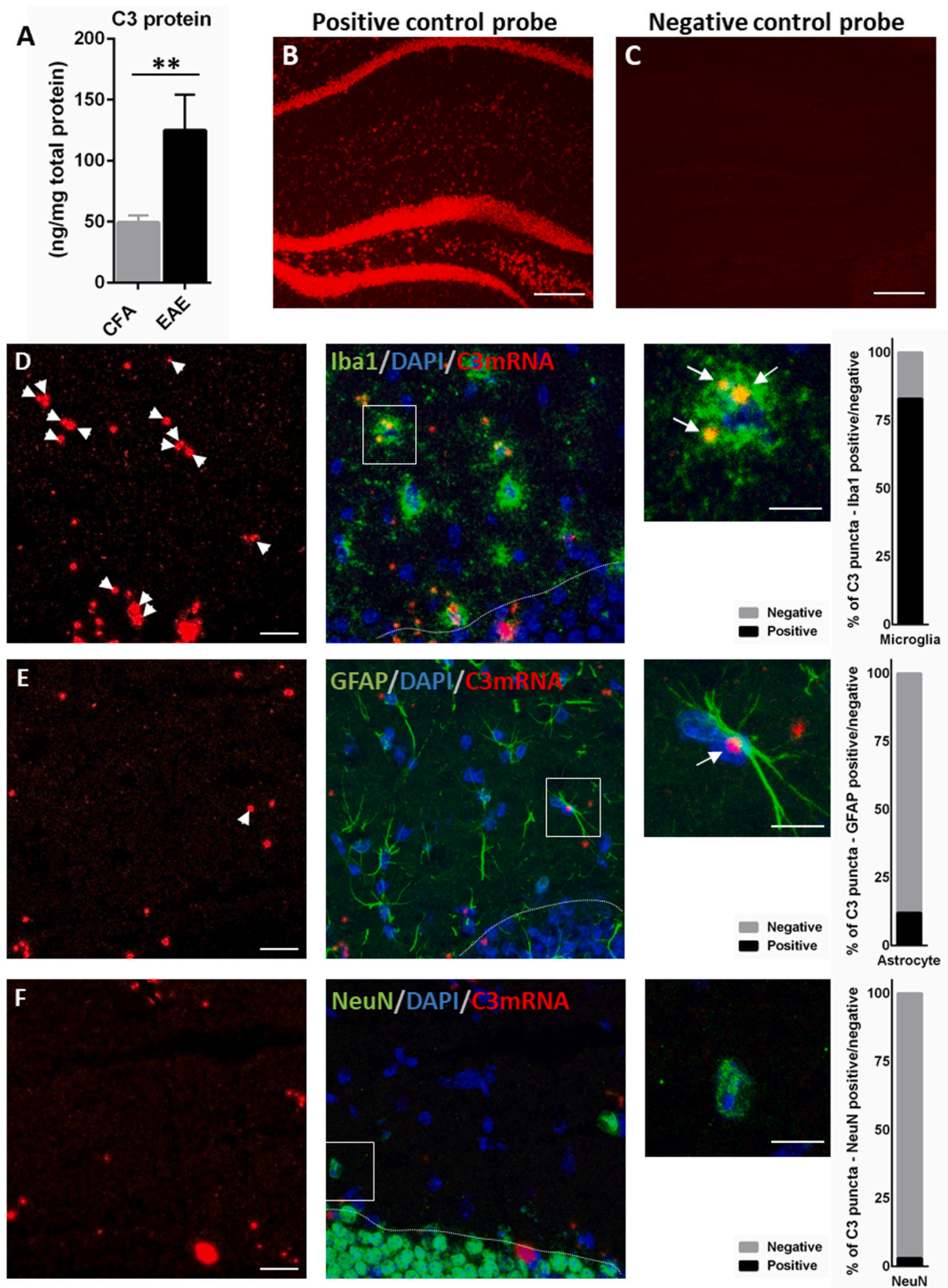
Fig. 2. Cellular origin of C3 in the dentate gyrus of EAE-mice.

(**A**) Content of C3 protein within the molecular layer of the dentate gyrus in EAE and CFA mice at 20 dpi. Error bars indicate mean ± SEM. EAE: $N = 8$ mice and CFA: $N = 8$ mice. ** $p \leq 0.01$ for Mann-Whitney test. (**B**) RNAscope positive control, conducted by using the control probe targeting the low-copy housekeeping gene *Ppib*, showed strong staining while RNAscope negative control (**C**), conducted by using the non-specific bacterial probe targeting *DapB* gene, showed no background. These controls ensured good quality of RNA and fixation conditions. (**D, E and F**) *In situ* hybridization of C3 mRNA (red) was combined with green immunofluorescence for markers of microglia (Iba1 in **D**), astrocyte (GFAP in **E**) and neuron (NeuN in **F**). Co-localizations are indicated with white arrows. Graphs show the percentages of C3 mRNA dots that were positive or negative for the considered cell type ($N = 4$ mice for each condition and $n = 4$ optical stacks per animal). Scale bar is 100 μm in B and C, 20 μm in D–F and 10 μm in zoomed images. The limit between the molecular layer of the dentate gyrus and the granular layer is showed in dotted lines. (For interpretation of the references to colour in this figure legend, the reader is referred to the web version of this article.)
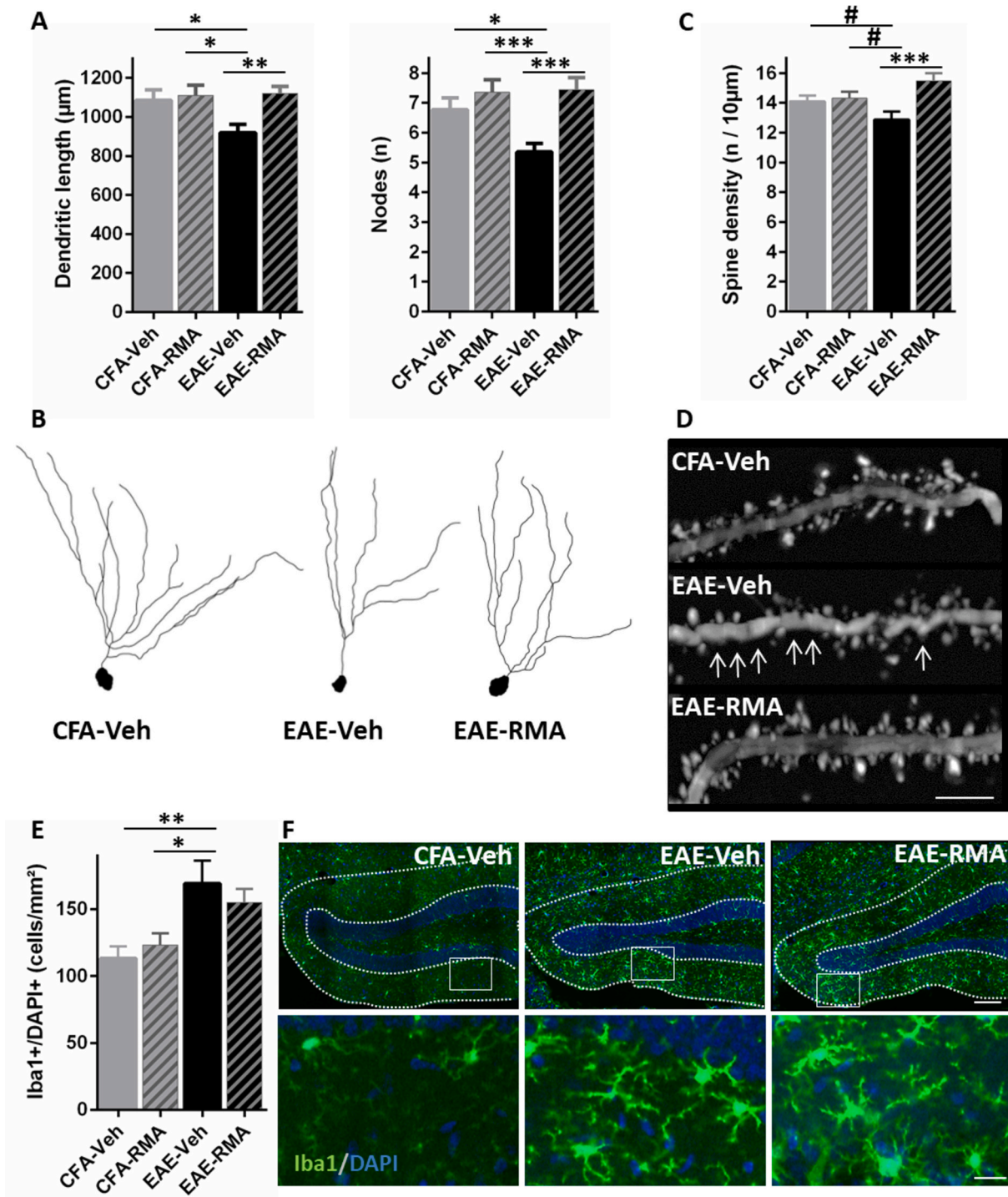
Fig. 3. Pharmacological inhibition of C3 prevents neuromorphological alterations in the dentate gyrus of EAE-mice.
(**A**) Morphometric analyses of the granule neurons of the dentate gyrus from Golgi staining in EAE and control CFA mice at 20 dpi which were treated by daily injections of RMA from 7 to 20 dpi (EAE-RMA and CFA-RMA) or by a vehicle solution (EAE-Veh and CFA-Veh; *n* = 25 to 29 neurons per groups from *N* = 5 to 8 mice per groups). (**B**) Representative examples of granule neurons of the dentate gyrus showing decreased total dendritic length and complexity in EAE-Veh mice. (**C**) Quantification of spines (counted on 54 to 61 dendrites per groups from N = 4 mice per groups) and (**D**) Representative examples from Golgi staining of dendrites showing domains devoid of spines in EAE-Veh (white arrows) but not in EAE-RMA. (**E**) Quantification of microglial cells number within the molecular layer of the dentate gyrus at 20 dpi (N = 5 mice per group and n = 4 regions of interest per mice). (**F**) Confocal images of microglial cells (Iba1, green) with blue nuclear counterstain (DAPI) showing signs of activation (stronger staining, thicker processes, more cells) in treated and untreated EAE-mice compared to CFA-mice. Images are displayed at low (top row) and higher magnification (bottom row) and the molecular layer of the dentate gyrus is outlined with dotted lines. Scale bar is 10 μm in D and 100 μm in F. Error bars indicate mean ± SEM. * $p < 0.05$, ** $p \leq 0.01$, *** $p \leq 0.001$ and # is for $0.05 < p < 0.10$ for one-way ANOVA and Tukey *post hoc*. (For interpretation of the references to colour in this figure legend, the reader is referred to the web version of this article.)

spines per 10 μm *vs.* 14.3 ± 0.43 spines per 10 μm, in EAE-Veh and CFA-Veh respectively, $p = 0.07$, one-way ANOVA and Tukey *post hoc*, Fig. 3C and D). In parallel, qualitative observations indicated that EAE-mice displayed strong modifications of microglial morphology with hypertrophied cell bodies and thicker processes, which classically reflect inflammatory activation state (Sierra et al., 2014). In addition, there was an increase in microglial density in EAE-mice compared to CFA-mice (169.1 ± 17.03 cells/mm^2 *vs.* 113.2 ± 9.12 cells/mm^2, in EAE-Veh, *N* = 5, and CFA-Veh, N = 5, respectively, $p < 0.01$, one-way ANOVA and Tukey *post hoc*, Fig. 3E and F). MBP and GFAP immunostaining did not reveal any overt modification of myelin and astrocyte structure respectively in EAE-mice compared to CFA-mice (**Supplemental Fig. 1**).

Daily i.p. injections of the C3 inhibitor RMA (Sahu et al., 1999) from 7 dpi to 20 dpi did not prevent EAE-induced motor symptoms, which were similar to those observed in untreated mice (**Supplemental Fig. 2**). Interestingly, EAE-RMA mice displayed a preservation of their dendritic length and complexity compared to EAE-Veh (1120 ± 35.8 μm *vs.* 919 ± 42.7 μm in length, $p < 0.01$ and 7.44 ± 0.40 nodes *vs.* 5.3 ± 0.28 nodes, in EAE-RMA and EAE-Veh respectively, $p < 0.001$, one-way ANOVA and Tukey *post hoc*, Fig. 3A and B) with values that were identical to those measured in CFA-mice. The number of dendritic spines was also preserved (15.4 ± 0.51 spines per 10 μm *vs.* 12.8 ± 0.55 spines per 10 μm, in EAE-RMA and EAE-Veh respectively, p < 0.001, one-way ANOVA and Tukey *post hoc*, Fig. 3C and D). The morphological changes of microglia that included larger soma and thicker primary processes and an increase of microglia density in EAE-RMA mice were identical to those in non-treated EAE-mice (155.0 ± 10.11 cells/mm^2 *vs.* 169.1 ± 17.03 cells/mm^2, in EAE-RMA and EAE-Veh respectively, $p = 0.77$, one-way ANOVA and Tukey *post hoc*, Fig. 3E and F) pointing to the fact that RMA does not have a widespread effect on inflammation and reactive gliosis. These data support the concept that C3 mediates dendritic and synaptic loss in response to EAE.

3.3. C3KO prevents dendritic loss in the dentate gyrus of EAE-mice

To circumvent potential off-targets of the RMA pharmacological approach (Habtemariam, 2018), we also investigated EAE-mediated hippocampus defects in C3KO mice with the same tools (*N* = 5 to 8). We observed that EAE was less severe in C3KO mice when compared to the wild type animals (**Supplemental Fig. 2**), as previously reported (Nataf et al., 2000; Szalai et al., 2007).

Morphometric analyses of dendrites of the granule neurons (*n* = 25 to 29 neurons per conditions from N = 5 to 8 mice) revealed that the knockout of C3 did not significantly impact dendritic length and complexity compared to WT mice at this age and under our sampling conditions (1152 ± 50.27 μm *vs.* 1114 ± 37.7 μm in length, p = ns and 7.7 ± 0.39 nodes *vs.* 7.1 ± 0.36 nodes, in CFA-C3KO and CFA-WT respectively, p = ns, one-way ANOVA and Tukey *post hoc*, Fig. 4A and B). Moreover, in line with previous findings (Wu et al., 2019), the knockout of C3 had no impact on spine density (13.8 ± 0.43 spines per 10 μm *vs.* 14.2 ± 0.39, in CFA-C3KO and CFA-WT respectively, p = ns, one-way ANOVA and Tukey *post hoc*, Fig. 4C and D). Finally, the dendritic alterations found in wild type EAE-mice were prevented when EAE was induced in the C3KO background (1146 ± 43.84 μm *vs.* 976 ± 54.08 μm in length, p < 0.01 and 7.3 ± 0.38 nodes *vs.* 5.8 ± 0.40 nodes, in EAE-C3KO and EAE-WT respectively, $p < 0.05$, one-way ANOVA and Tukey *post hoc*, Fig. 4A and B), and spine density was similarly preserved to normal levels (13.8 ± 0.40 spines per 10 μmin *vs.* 12.1 ± 0.53, in EAE-C3KO and EAE-WT respectively, $p < 0.05$, one-way ANOVA and Tukey *post hoc*, Fig. 4C and D).

These data further argue for an involvement of C3 in the hippocampal dendritic and synaptic alterations observed in the early stage of EAE. However, it is important to consider that EAE-C3KO mice showed only a moderate and non-significant increase of microglia density (134.2 ± 8.18 cells/mm^2 *vs.* 115.3 ± 6.97 cells/mm^2, in EAE-C3KO and CFA-C3KO respectively, $p = 0.60$, one-way ANOVA and Tukey *post hoc*)

that was significantly inferior to the microglia density observed in EAE-WT (134.2 ± 8.18 cells/mm^2 *vs.* 180.8 ± 22.16 cells/mm^2, in EAE-C3KO and EAE-WT respectively, $p = 0.02$, one-way ANOVA and Tukey *post hoc*, Fig. 4E and F).

### 3.4. C3 inhibitor and C3KO prevent microglia phagocytosis

C3KO alters all the downstream products including C3a and C3b while RMA is known to inhibit more specifically the action of C3b (Sahu et al., 1999). C3b can opsonize elements to be eliminated by microglia, the latter being the only resident brain cells to express the C3b receptor called CR3 (Stephan et al., 2012; Hong et al., 2016; Schafer et al., 2012) (Fig. 1B and C). As mRNA for the two CR3 subunits were increased in EAE (Fig. 1D), we assessed microglial engulfment of the post-synaptic protein Homer in CD68-positive lysosomes by 3D reconstruction of confocal z stacks (N = 5 mice per group and 30-to-49 microglia per group). The number of lysosomial homer puncta in microglial cells was significantly higher in EAE-mice compared to CFA-mice (*n* = 36.0 ± 5.37 homer puncta per microglia in EAE-Veh *vs.* *n* = 18.2 ± 2.06, *n* = 17.0 ± 1.91, and *n* = 16.4 ± 2.41, in CFA-Veh, CFA-RMA and CFA-C3KO respectively, $p = 0.024$, $p = 0.013$ and $p = 0.009$, Kruskal-Wallis test and FDR correction, Fig. 5). Both EAE-RMA and EAE-C3KO mice showed decreased numbers of homer puncta within microglia cells compared to EAE-Veh (*n* = 20.6 ± 3.33 homer puncta per microglia in EAE-RMA and *n* = 19.2 ± 3.85 homer puncta per microglia in EAE-C3KO *vs.* n = 36.0 ± 5.37, in EAE-Veh, $p = 0.029$ and $p = 0.018$ respectively, Kruskal-Wallis test and FDR correction, Fig. 5). These data suggest that hippocampal dendritic and synaptic loss in EAE is mediated by microglial phagocytosis through a complement-dependent mechanism.

3.5. Disruption of the complement cascade prevents memory deficit in EAE-mice

The pharmacological and the transgenic approach have reduced the C3-mediated dendritic loss, synaptic loss and phagocytic activity, which could reflect either *(i)* blocking a beneficial removal of dying or altered neuronal elements, or *(ii)* blocking a detrimental removal of viable neuronal elements. To unravel the functional impact of disrupting the complement cascade in EAE mice, we assessed their memory abilities in a contextual fear conditioning protocol (Fig. 6A).

After re-exposure to the predictive context, mice spent around 30-to-50% of the time exhibiting conditioned freezing with an expected progressive extinction over time as no shock was delivered the day of testing. During the first 2 min of such re-exposure to the predictive context, EAE-mice showed significantly less conditioned freezing than CFA-mice (freezing rate = 32.7 ± 2.51% *vs.* 45.4 ± 4.23%, in EAE-Veh and CFA-Veh respectively, $p < 0.05$, one-way ANOVA and Tukey *post hoc*, Fig. 6B). Moreover when the same mice were re-exposed to the tone alone, an irrelevant stress-related stimulus (not predicting the threat), CFA-mice showed no fear response to the tone while EAE-mice exhibited a paradoxical (abnormally high) freezing behavior to the tone compared to pre- and post-exposure period. This translated into a significantly higher freezing ratio in EAE-mice compared to CFA-mice (freezing ratio = 0.18 ± 0.02 *vs.* 0.07 ± 0.02, in EAE-Veh and CFA-Veh respectively, $p < 0.01$, one-way ANOVA and Tukey *post hoc*, Fig. 6B). Altogether this behavioral profile is likely to result from the hippocampal alterations described above, as functional integrity of the hippocampus is crucial for contextual memory (Desmedt et al., 2015; Kaouane et al., 2012) while the maladaptive response to the tone has been repeatedly shown to reflect an amygdala-dependent conditioning to one of the most salient and simple cues (the tone) to compensate for the hippocampal deficiency to form the complex representation of contextual information (Kaouane et al., 2012; Desmedt et al., 2015; Planche et al., 2017a; Calandreau et al., 2006).

Interestingly, RMA-treated EAE mice showed a higher conditioned fear response to the predictive conditioning context compared to
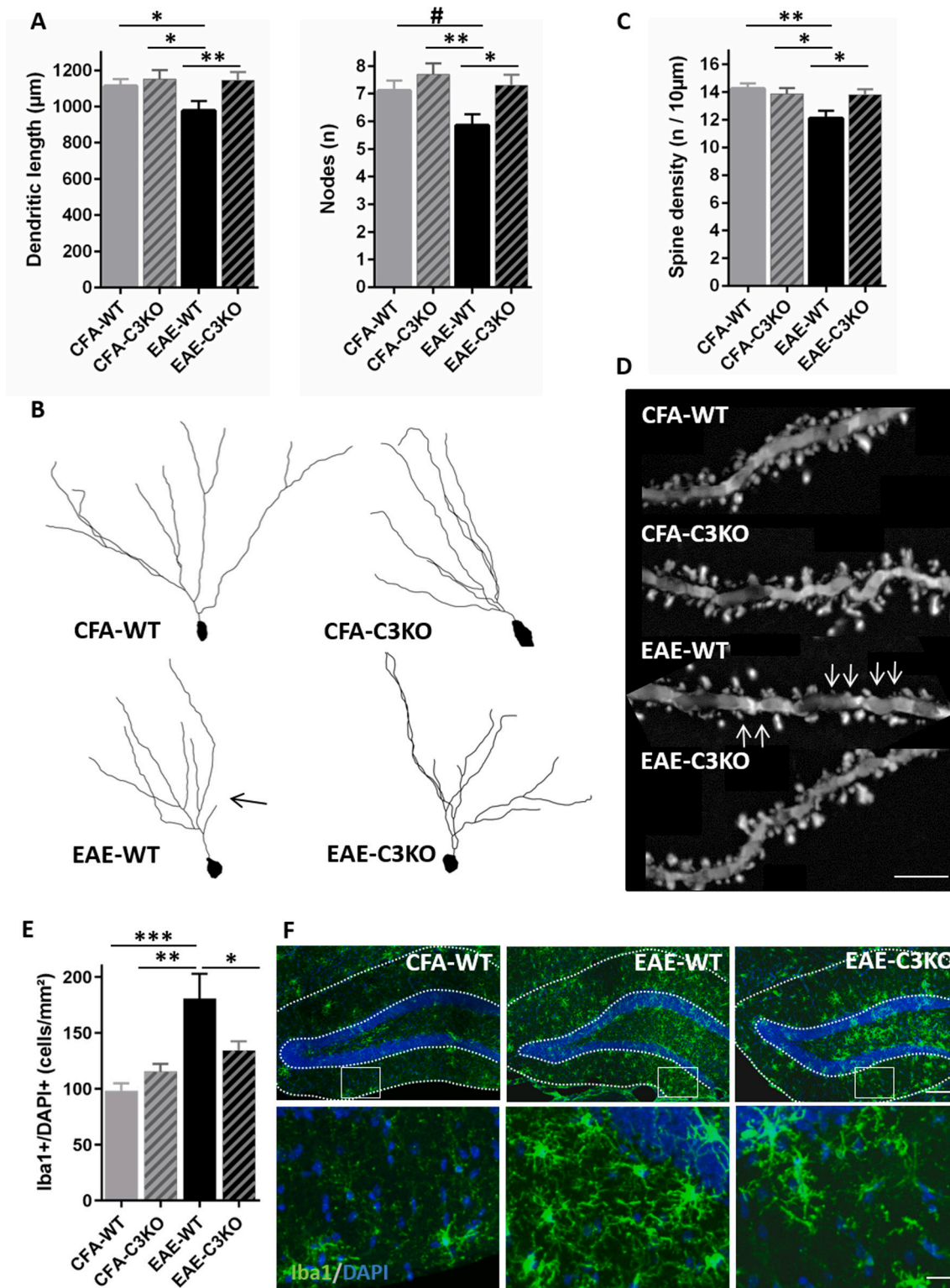
Fig. 4. Effect of C3KO on neuromorphological alterations in the dentate gyrus of EAE-mice.
(**A**) Morphometric analyses of the granule neurons of the dentate gyrus from Golgi staining in EAE and control CFA mice at 20 dpi which were induced on the C57BL6/j wild type background (EAE-WT and CFA-WT) or on the C3 knock-out background (EAE-C3KO and CFA-C3KO; n = 25 to 29 neurons per groups from N = 5 to 8 mice per groups). (**B**) Representative examples of granule neurons of the dentate gyrus showing decreased total dendritic length and complexity in EAE-WT mice with typical interruption of dendrites (arrow) that were preserved in EAE-C3KO. (**C**) Quantification of spines (counted on 54 to 61 dendrites per groups from N = 4 mice per groups) and (**D**) representative examples from Golgi staining of dendrite showing domains devoid of spines in EAE-WT (white arrows) but not in EAE-C3KO. (**E**) Quantification of microglial cells number within the molecular layer of the dentate gyrus at 20 dpi (N = 5 mice per group and n = 4 regions of interest per mice). (**F**) Confocal images of microglial cells (Iba1, green) with blue nuclear counterstain (DAPI) showing only moderate sign of activation in EAE-C3KO. Images are displayed at low (top row) and higher magnification (bottom row) and the molecular layer of the dentate gyrus is outlined with dotted lines. Scale bar is 10 μm in D and 100 μ in F. Error bars indicate mean ± SEM. * p < 0.05, ** p ≤ 0.01, *** p ≤ 0.001 and # is for *p* = 0.056 for one-way ANOVA and Tukey *post hoc*. (For interpretation of the references to colour in this figure legend, the reader is referred to the web version of this article.)
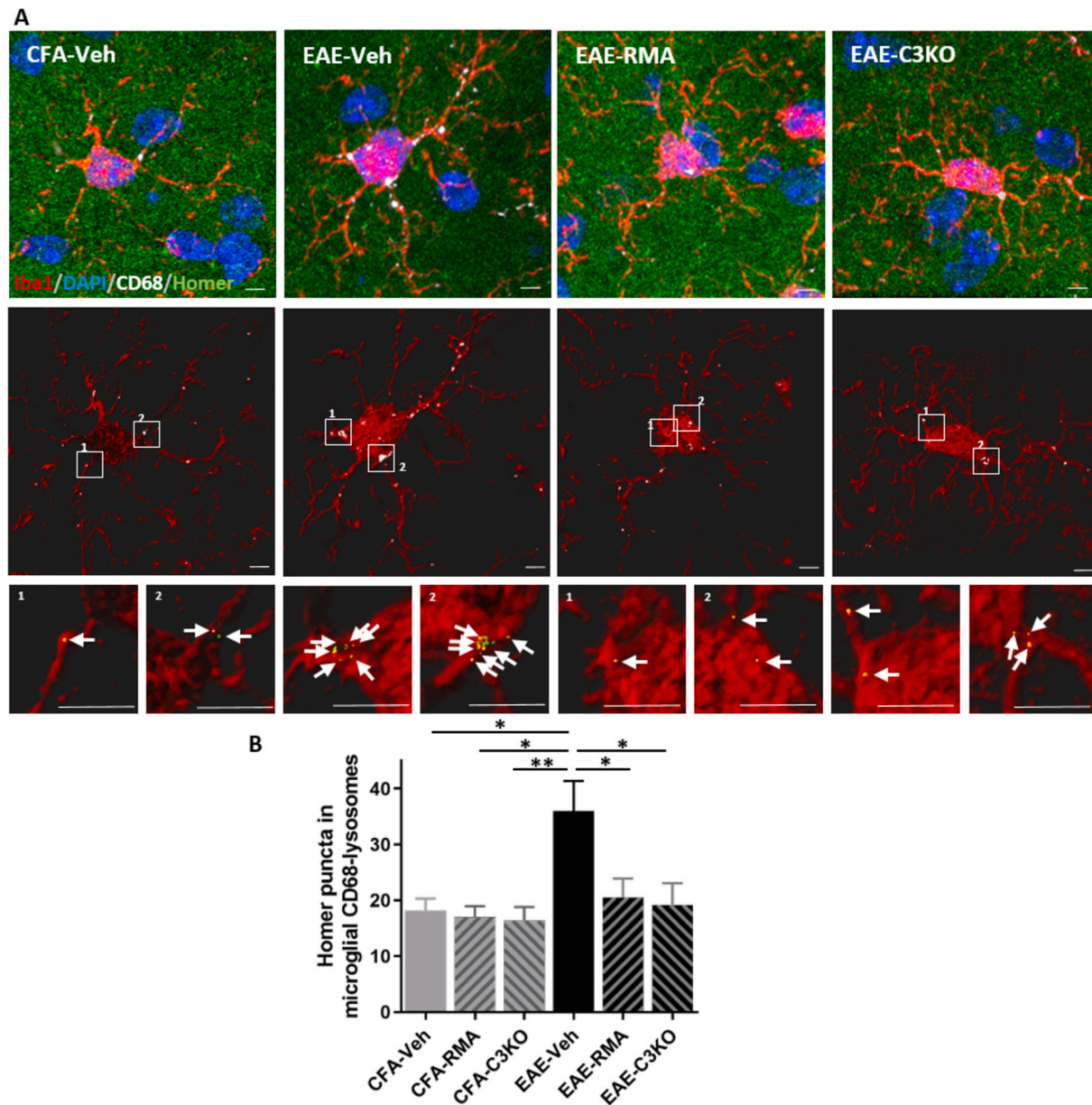
Fig. 5. C3KO and pharmacological inhibition of C3 prevent microglial synapse engulfment in the dentate gyrus of EAE-mice.
(**A**) Immunostaining of microglial cells (Iba1, red) with blue nuclear counterstain (DAPI), lysosomes (CD68, grey) and synapses (Homer, green) are shown as raw confocal images (top), as 3D isosurface reconstruction of microglial cells together with lysosomes located inside microglial cells (middle), and as homer puncta (bottom) inside lysosomes in two enlarged illustrative locations (right). Scale bar is 8 μm (**B**) Quantification of Homer puncta in CD68 lysosomes per microglia. Number of microglia analyzed per group = 30-to-49 from N = 5 mice per group. Error bars indicate mean ± SEM. * $p < 0.05$ and ** $p \leq 0.01$ for Kruskal-Wallis test and FDR correction. (For interpretation of the references to colour in this figure legend, the reader is referred to the web version of this article.)

vehicle-treated EAE mice (freezing rate = 42.8 ± 2.17% *vs.* 32.7 ± 2.51%, in EAE-RMA and EAE-Veh respectively, $p < 0.05$, one-way ANOVA and Tukey *post hoc*, Fig. 6B) and a lower fear response to the non-predictive tone (freezing ratio = 0.09 ± 0.02 *vs.* 0.18 ± 0.02, in EAE-RMA and EAE-Veh respectively, $p < 0.05$, one-way ANOVA and Tukey *post hoc*, Fig. 6B) demonstrating that RMA could prevent the early memory impairment observed in EAE-mice. The protective effect observed after the pharmacological inhibition of C3 was also confirmed in C3KO mice (Fig. 6C). Altogether this indicates that C3 is involved in hippocampal alterations and impacts memory performances in EAE.

4. Discussion

In this study, we provided further arguments for a role of the complement cascade central component, C3, in synaptic and dendritic alterations within the dentate gyrus which drives memory deficit at the early stage of experimental MS.

Cognitive impairment is recognized as a core feature of MS and has a negative impact on daily activities (Chiaravalloti and DeLuca, 2008). The pathogenesis of MS-related cognitive impairment is multi-factorial entangling dysfunctions in both white matter and grey matter, in relation with both inflammatory and neurodegenerative components of the disease (Di Filippo et al., 2018). Indeed, white matter lesions, which are inflammatory and demyelinating lesions caused by penetration of autoreactive T cells from the bloodstream (Compston and Coles, 2008), have been linked to cognitive deficits such as reduction of information processing speed as a result of disconnection of networks (Dineen et al., 2009). Grey matter alterations also emerged as major contributors
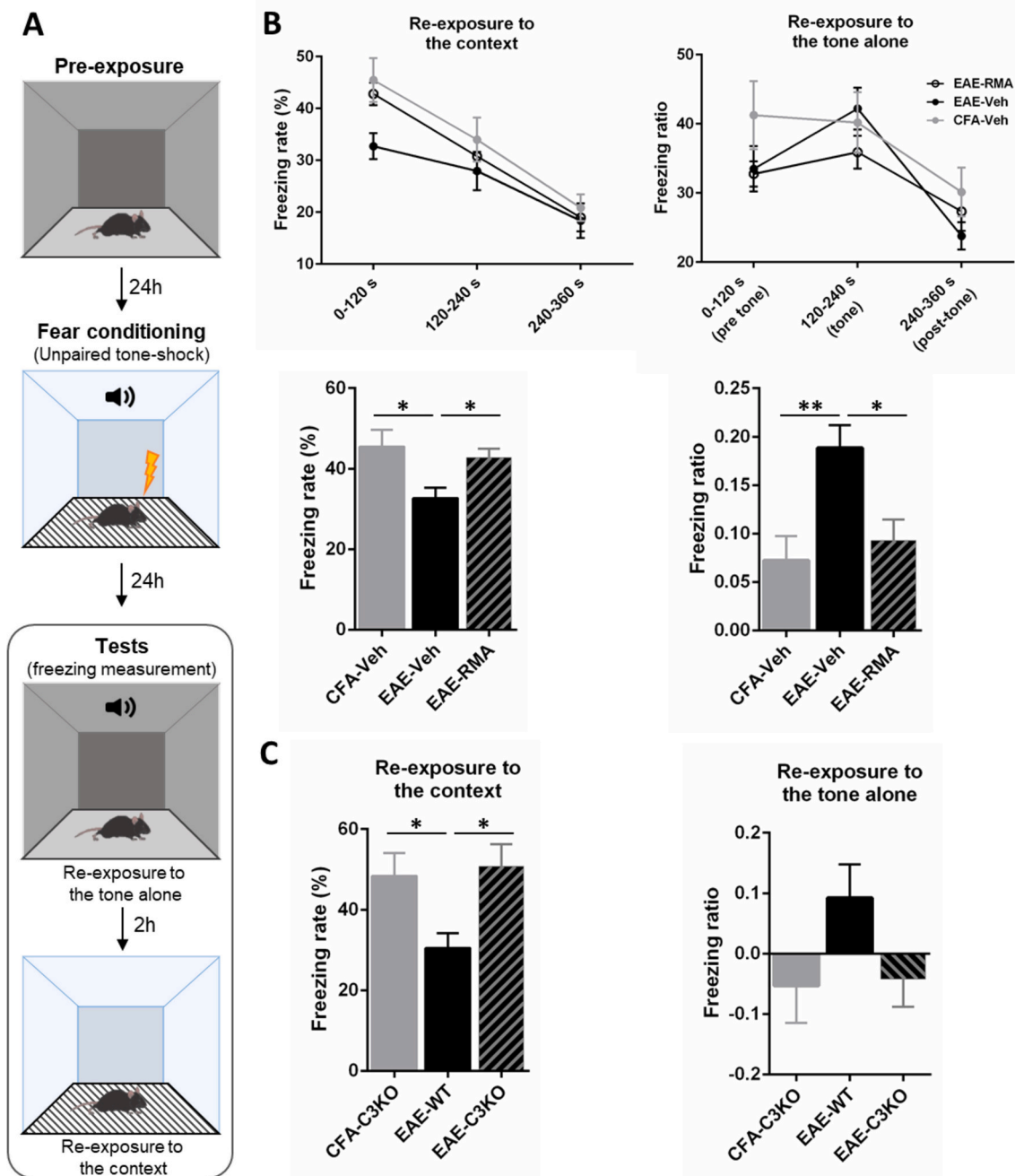
Fig. 6. Deletion of C3, either pharmacologically or by a transgenic approach, preserved memory abilities in EAE-mice.
(**A**) Representation of the contextual fear conditioning paradigm in which the context is the only predictor of the footshock while the discrete tone is not (pseudo-random distribution of tone and footshock that are unpaired). (**B**) Comparison of EAE, control CFA and EAE treated with RMA ($N = 15$ mice per group). Freezing rate is plotted over time when mice were re-exposed to the context or to the tone alone in a safe and familiar environment. From these evolutions, the freezing rate over the first 2 min of re-exposition to the context is plotted as well as the freezing ratio that quantifies the differential freezing to the tone compared to the pre- and post-tone period. (**C**) Comparison of EAE, CFA and EAE induced in the C3KO background ($N = 13$ to 18 mice per group). Error bars indicate mean $\pm$ SEM. * $p < 0.05$, ** $p \leq 0.01$ for one-way ANOVA and Tukey *post hoc*.

(Calabrese et al., 2015) with particular relevance of key structures such as hippocampus for memory performances (Sicotte et al., 2008). In grey matter, inflammatory elements (and notably pro-inflammatory cytokines) have been linked to synaptic dysfunctions and plasticity alterations (Di Filippo et al., 2013; Habbas et al., 2015; Mandolesi et al., 2015). Synaptic loss and dendritic degeneration have also been reported (in hippocampus and other grey matter regions) both in post-mortem brain of MS patients (Dutta et al., 2011; Jurgens et al., 2016) and in EAE model (Ziehn et al., 2012; Ziehn et al., 2010; Planche et al., 2017a), highlighting an important role for a neurodegenerative component.

Elucidating the mechanisms involved in early grey matter neuro-degeneration in MS is of particular interest to avoid irreversible alterations and to preserve cognitive functions. Intensive researches have investigated possible inter-relations between inflammation and neuro-degeneration. One pathway could involve perturbation of synaptic homeostasis by inflammatory cells leading to excitotoxic damages and ultimately synaptic loss (Mandolesi et al., 2015). In this paper, we highlighted another pathway linking the inflammation-related microglia activation to early synaptic and dendritic loss through the complement component C3. Importantly, to address the memory impact of

such pathway in EAE, careful behavioral paradigm should be designed to avoid bias related to sensory-motor impairment. In that sense, in our unpaired tone-shock contextual conditioning paradigm, the improper conditioning of mice to the non-predictive tone ensured that fear learning was not impacted by sensory-motor, and further supported the hippocampal deficiency through previously reported phenomenon of amygdala compensation (Calandreau et al., 2006; Kaouane et al., 2012; Desmedt et al., 2015; Planche et al., 2017a). This interpretation implies preservation of the amygdala, an area where microglia was indeed reported not to be activated in early EAE, even displaying an increased synaptic activity (Acharjee et al., 2018) in accordance with the concept of region-dependent microglial diversity (Grabert et al., 2016).

Microglia are rapidly activated in response to inflammation induced by autoreactive T cells in EAE (Heppner et al., 2005) and in MS patients (Colasanti et al., 2016). As professional phagocytes, microglia can engulf synapses, dendrites or even whole neurons. In MS, phagocytosis can remove dead cells and myelin debris - the so-called secondary phagocytosis - that has been well described and that is potentially helpful for remyelination (Aguzzi et al., 2013). If such secondary phagocytosis had been relevant in our model, we would have expected worsening the disease through its inhibition. Here, we point toward another process, the primary phagocytosis of viable neuronal elements by microglia, because its inhibition protected against dendritic and synaptic loss, and ultimately preserved memory performances. However, it is possible that this noxious process, highlighted here in the early stage of the disease can also be balanced by more beneficial phagocytosis that may take place in later stages, when demyelination becomes predominant. Longitudinal data will be required to test this hypothesis. The cross-talk between microglia and neurons can involve different signals, opsonins and receptors depending on the specific pathophysiological context (Brown and Neher, 2014). It is interesting to note that among the most common signaling pathways implicated in microglia-neuron interaction, we found that only the complement components were upregulated. While this doesn't fully rule out the possible implication of the other pathways that could be involved without any up- or down-regulation of their components at the mRNA level, this highlights the predominant role of the complement in the neurodegenerative part of MS triggered by microglia activation.

In MS, activation of the complement cascade has been described for a long time in inflammatory white matter lesions; the cascade up to the terminal component C5b-C9 participates to demyelination (Ingram et al., 2014). It is important to note that C5 was not increased in our analyses of the dentate gyrus, in line with pathological data in human hippocampus (Michailidou et al., 2015), suggesting no activation downstream of C3 such as the inflammatory C5a-C5aR axis or the terminal C5b9 complex. These data are consistent with location-dependent differential activation of the complement, that is part of the inflammatory cascade in white matter lesions, but not in grey matter (Brink et al., 2005). In the hippocampus, a grey matter structural component, we point toward an active neurodegenerative process mediated by activated microglia through partial activation of the complement, similarly to what has been described for synaptic pruning during development (Stevens et al., 2007; Schafer et al., 2012). During development, neuronal projections are refined *via* the elimination of numerous synapses to transform immature circuits into organized adult networks which involves the tagging of the supernumerary synapses by C1, their opsonization by C3b and phagocytosis by microglia *via* CR3 (Stevens et al., 2007; Schafer et al., 2012). Several papers already provided data for an aberrant reactivation of this complement pathway participating to synaptic loss in Alzheimer's disease (Wu et al., 2019; Hong et al., 2016; Hansen et al., 2018; Shi et al., 2017), glaucoma (Stevens et al., 2007; Howell et al., 2011) or frontotemporal dementia (Lui et al., 2016). Here, we add to the new field indicating that the neurodegenerative component of MS, within grey matter, could also share similarities with these other neurodegenerative diseases in lines with two recent publications. Werneburg et al. (2020) were the first to report C3-dependent synaptic

loss in MS (in both post-mortem tissues and animal models) within the lateral geniculate nucleus, a grey matter relay of the visual system. We extend this finding to the hippocampus, providing additional elements to the first hippocampal analyses conducted by Hammond et al. (2020) which points toward a general mechanism of grey matter dysfunction in MS. However there are specificities to MS as we identified microglia/myeloid cells as the main source of C3, while reactive astrocytes were pointed as the source of C3 after induction by microglia in other conditions (Liddelow et al., 2017). This is consistent and complementary to Hammond et al. (2020) data who reported strong C3 mRNA increase within CD11b + cells isolated from the hippocampus (and cortex) of EAE mice but without exploration of other cell types. Microglial cells can actually produce C3 similarly to astrocytes and it is believed that the production could be disease-specific (microglia also produced significant C3 in a mouse model of tauopathy (Wu et al., 2019)) and time-dependent. It is important to say that we found no reactive astrocytes in our study because we were focusing in early stage but reactive astrocytes have been reported at later stages (Ludwin et al., 2016) and further studies should investigate whether astrocytes could also participate to C3 synthesis together with microglia at later stages of MS.

We have to acknowledge that manipulating C3 in EAE is difficult because the complement cascade is also participating to the induction of the disease itself (Szalai et al., 2007; Nataf et al., 2000). Indeed, C3KO mice developed an attenuated form of EAE compared to wild-type littermates (lower motor scores), which is attributed from the literature to a reduced infiltration of CD4$^+$ and CD8$^+$ T cells (Nataf et al., 2000; Szalai et al., 2007) due to a deficit in the chemoattractant C3a that is downstream C3 (Boos et al., 2004). Therefore, from C3KO mice data alone, it is difficult to conclude formally that the neuroprotection is specifically related to the defect in C3b-CR3 interaction rather than to the overall reduction of inflammation (Hammond et al., 2020). Our parallel C3KO and pharmacological approaches with RMA using the same tools provides important complementary data because RMA was described to act on the C3b pathway (Sahu et al., 1999). As a result, EAE-mice treated with RMA developed a disease of similar motor severity and with similar number of microglia cells compared to wild type animals, but the neuroprotective central effect of RMA treatment was also clearly apparent. This is suggestive of a specific contribution of C3 in the neurodegenerative process on top of its contribution in the global inflammatory cascade even though RMA can have pleiotropic effects (Habtemariam, 2018). Future experiments to locally and cell-specifically inhibit C3 in the hippocampus could provide new insights. Even with these caveats in mind, our current data, synergistically with the others (Werneburg et al., 2020; Hammond et al., 2020), highlight a mechanistic pathway for neurodegeneration in EAE that echoes the increase of complement factors found in the hippocampus of MS patients from post-mortem pathological studies (Michailidou et al., 2015; Watkins et al., 2016). It is also interesting that we report such mechanisms in the dentate gyrus at the peak of the first relapse in line with the early vulnerability of this subfield (Planche et al., 2017a; Planche et al., 2017b; Habbas et al., 2015) while Hammond et al. (2020) also found similar data in CA1 at a later stage which agree with the dynamic spreading of atrophy from dentate gyrus to CA1 that we highlighted in humans with *in vivo* imaging (Planche et al., 2018). Future experiments should address the time course of this process including analyses at earlier time-points because microglia was found rapidly activated in the hippocampus of EAE mice (Habbas et al., 2015).

To summarize, we provide evidences for a microglial, C3-dependent, neurodegenerative process in the dentate gyrus, that is responsible for memory impairment in early phase of MS and that can be prevented pharmacologically by RMA. These findings echo, at some levels, mechanisms observed in other neurodegenerative conditions and pave the way toward therapeutic perspectives by manipulating the complement system.

Declaration of Competing Interest

None.

Acknowledgments

Appendix A. Supplementary data

Supplementary data to this article can be found online at https://doi.org/10.1016/j.nbd.2021.105533.

References

Acharjee, S., Nayani, N., Tsutsui, M., Hill, M.N., Ousman, S.S., Pittman, Q.J., 2013. Altered cognitive-emotional behavior in early experimental autoimmune encephalitis–cytokine and hormonal correlates. Brain Behav. Immun. 33, 164–172.

Acharjee, S., Verbeek, M., Gomez, C.D., Bisht, K., Lee, B., Benoit, L., Sharkey, K.A., Benediktsson, A., Tremblay, M.E., Pittman, Q.J., 2018. Reduced microglial activity and enhanced glutamate transmission in the Basolateral amygdala in early CNS autoimmunity. J. Neurosci. 38, 9019–9033.

Aguzzi, A., Barres, B.A., Bennett, M.L., 2013. Microglia: scapegoat, saboteur, or something else? Science 339, 156–161.

Baxter, A.G., 2007. The origin and application of experimental autoimmune encephalomyelitis. Nat. Rev. Immunol. 7, 904–912.

Boos, L., Campbell, I.L., Ames, R., Wetsel, R.A., Barnum, S.R., 2004. Deletion of the complement anaphylatoxin C3a receptor attenuates, whereas ectopic expression of C3a in the brain exacerbates, experimental autoimmune encephalomyelitis. J. Immunol. 173, 4708–4714.

Brink, B.P., Veerhuis, R., Breij, E.C., van der Valk, P., Dijkstra, C.D., Bo, L., 2005. The pathology of multiple sclerosis is location-dependent: no significant complement activation is detected in purely cortical lesions. J. Neuropathol. Exp. Neurol. 64, 147–155.

Brown, G.C., Neher, J.J., 2014. Microglial phagocytosis of live neurons. Nat. Rev. Neurosci. 15, 209–216.

Bustin, S.A., Benes, V., Garson, J.A., Hellemans, J., Huggett, J., Kubista, M., Mueller, R., Nolan, T., Pfaffl, M.W., Shipley, G.L., Vandesompele, J., Wittwer, C.T., 2009. The MIQE guidelines: minimum information for publication of quantitative real-time PCR experiments. Clin. Chem. 55, 611–622.

Calabrese, M., Magliozzi, R., Ciccarelli, O., Geurts, J.J., Reynolds, R., Martin, R., 2015. Exploring the origins of grey matter damage in multiple sclerosis. Nat. Rev. Neurosci. 16, 147–158.

Calandreau, L., Trifilieff, P., Mons, N., Costes, L., Marien, M., Marighetto, A., Micheau, J., Jaffard, R., Desmedt, A., 2006. Extracellular hippocampal acetylcholine level controls amygdala function and promotes adaptive conditioned emotional response. J. Neurosci. 26, 13556–13566.

Chiaravalloti, N.D., DeLuca, J., 2008. Cognitive impairment in multiple sclerosis. Lancet Neurol. 7, 1139–1151.

Colasanti, A., Guo, Q., Giannetti, P., Wall, M.B., Newbould, R.D., Bishop, C., Onega, M., Nicholas, R., Ciccarelli, O., Muraro, P.A., Malik, O., Owen, D.R., Young, A.H., Gunn, R.N., Piccini, P., Matthews, P.M., Rabiner, E.A., 2016. Hippocampal neuroinflammation, functional connectivity, and depressive symptoms in multiple sclerosis. Biol. Psychiatry 80, 62–72.

Compston, A., Coles, A., 2008. Multiple sclerosis. Lancet 372, 1502–1517.

Crombe, A., Planche, V., Raffard, G., Bourel, J., Dubourdieu, N., Panatier, A., Fukutomi, H., Dousset, V., Oliet, S., Hiba, B., Tourdias, T., 2018. Deciphering the microstructure of hippocampal subfields with in vivo DTI and NODDI: applications to experimental multiple sclerosis. Neuroimage 172, 357–368.

Dejanovic, B., Huntley, M.A., De Maziere, A., Meilandt, W.J., Wu, T., Srinivasan, K., Jiang, Z., Gandham, V., Friedman, B.A., Ngu, H., Foreman, O., Carano, R.A.D., Chih, B., Klumperman, J., Bakalarski, C., Hanson, J.E., Sheng, M., 2018. Changes in the synaptic proteome in Tauopathy and Rescue of tau-Induced Synapse Loss by C1q antibodies. Neuron 100 (1322–36), e7.

Desmedt, A., Marighetto, A., Richter-Levin, G., Calandreau, L., 2015. Adaptive emotional memory: the key hippocampal-amygdalar interaction. Stress 18, 297–308.

Di Filippo, M., Chiasserini, D., Gardoni, F., Viviani, B., Tozzi, A., Giampa, C., Costa, C., Tantucci, M., Zianni, E., Boraso, M., Siliquini, S., de Iure, A., Ghiglieri, V., Colcelli, E., Baker, D., Sarchielli, P., Fusco, F.R., Di Luca, M., Calabresi, P., 2013. Effects of central and peripheral inflammation on hippocampal synaptic plasticity. Neurobiol. Dis. 52, 229–236.

Di Filippo, M., de Iure, A., Giampa, C., Chiasserini, D., Tozzi, A., Orvietani, P.L., Ghiglieri, V., Tantucci, M., Durante, V., Quiroga-Varela, A., Mancini, A., Costa, C., Sarchielli, P., Fusco, F.R., Calabresi, P., 2016. Persistent activation of microglia and NADPH oxidase [corrected] drive hippocampal dysfunction in experimental multiple sclerosis. Sci. Rep. 6, 20926.

Di Filippo, M., Portaccio, E., Mancini, A., Calabresi, P., 2018. Multiple sclerosis and cognition: synaptic failure and network dysfunction. Nat. Rev. Neurosci. 19, 599–609.

Dineen, R.A., Vilisaar, J., Hlinka, J., Bradshaw, C.M., Morgan, P.S., Constantinescu, C.S., Auer, D.P., 2009. Disconnection as a mechanism for cognitive dysfunction in multiple sclerosis. Brain 132, 239–249.

Dutta, R., Chang, A., Doud, M.K., Kidd, G.J., Ribaudo, M.V., Young, E.A., Fox, R.J., Staugaitis, S.M., Trapp, B.D., 2011. Demyelination causes synaptic alterations in hippocampi from multiple sclerosis patients. Ann. Neurol. 69, 445–454.

Feuillet, L., Reuter, F., Audoin, B., Malikova, I., Barrau, K., Cherif, A.A., Pelletier, J., 2007. Early cognitive impairment in patients with clinically isolated syndrome suggestive of multiple sclerosis. Mult. Scler. 13, 124–127.

Grabert, K., Michael, T., Karavolos, M.H., Clohisey, S., Baillie, J.K., Stevens, M.P., Freeman, T.C., Summers, K.M., McColl, B.W., 2016. Microglial brain region-dependent diversity and selective regional sensitivities to aging. Nat. Neurosci. 19, 504–516.

Habbas, S., Santello, M., Becker, D., Stubbe, H., Zappia, G., Liaudet, N., Klaus, F.R., Kollias, G., Fontana, A., Pryce, C.R., Suter, T., Volterra, A., 2015. Neuroinflammatory TNFalpha impairs memory via astrocyte signaling. Cell 163, 1730–1741.

Habtemariam, S., 2018. Molecular pharmacology of rosmarinic and salvianolic acids: potential seeds for Alzheimer's and vascular dementia drugs. Int. J. Mol. Sci. 19.

Haji, N., Mandolesi, G., Gentile, A., Sacchetti, L., Fresegna, D., Rossi, S., Musella, A., Sepman, H., Motta, C., Studer, V., De Chiara, V., Bernardi, G., Strata, P., Centonze, D., 2012. TNF-alpha-mediated anxiety in a mouse model of multiple sclerosis. Exp. Neurol. 237, 296–303.

Hammond, J.W., Bellizzi, M.J., Ware, C., Qiu, W.Q., Saminathan, P., Li, H., Luo, S., Ma, S.A., Li, Y., Gelbard, H.A., 2020. Complement-dependent synapse loss and microgliosis in a mouse model of multiple sclerosis. Brain Behav. Immun. 87, 739–750.

Hansen, D.V., Hanson, J.E., Sheng, M., 2018. Microglia in Alzheimer's disease. J. Cell Biol. 217, 459–472.

Heppner, F.L., Greter, M., Marino, D., Falsig, J., Raivich, G., Hovelmeyer, N., Waisman, A., Rulicke, T., Prinz, M., Priller, J., Becher, B., Aguzzi, A., 2005. Experimental autoimmune encephalomyelitis repressed by microglial paralysis. Nat. Med. 11, 146–152.

Hong, S., Beja-Glasser, V.F., Nfonoyim, B.M., Frouin, A., Li, S., Ramakrishnan, S., Merry, K.M., Shi, Q., Rosenthal, A., Barres, B.A., Lemere, C.A., Selkoe, D.J., Stevens, B., 2016. Complement and microglia mediate early synapse loss in Alzheimer mouse models. Science 352, 712–716.

Howell, G.R., Macalinao, D.G., Sousa, G.L., Walden, M., Soto, I., Kneeland, S.C., Barbay, J.M., King, B.L., Marchant, J.K., Hibbs, M., Stevens, B., Barres, B.A., Clark, A.F., Libby, R.T., John, S.W., 2011. Molecular clustering identifies complement and endothelin induction as early events in a mouse model of glaucoma. J. Clin. Invest. 121, 1429–1444.

Ingram, G., Loveless, S., Howell, O.W., Hakobyan, S., Dancey, B., Harris, C.L., Robertson, N.P., Neal, J.W., Morgan, B.P., 2014. Complement activation in multiple sclerosis plaques: an immunohistochemical analysis. Acta Neuropathol. Commun. 2, 53.

Jurgens, T., Jafari, M., Kreutzfeldt, M., Bahn, E., Bruck, W., Kerschensteiner, M., Merkler, D., 2016. Reconstruction of single cortical projection neurons reveals primary spine loss in multiple sclerosis. Brain 139, 39–46.

Kaouane, N., Porte, Y., Vallee, M., Brayda-Bruno, L., Mons, N., Calandreau, L., Marighetto, A., Piazza, P.V., Desmedt, A., 2012. Glucocorticoids can induce PTSD-like memory impairments in mice. Science 335, 1510–1513.

Konsman, J.P., Parnet, P., Dantzer, R., 2002. Cytokine-induced sickness behaviour: mechanisms and implications. Trends Neurosci. 25, 154–159.

Liddelow, S.A., Guttenplan, K.A., Clarke, L.E., Bennett, F.C., Bohlen, C.J., Schirmer, L., Bennett, M.L., Munch, A.E., Chung, W.S., Peterson, T.C., Wilton, D.K., Frouin, A., Napier, B.A., Panicker, N., Kumar, M., Buckwalter, M.S., Rowitch, D.H., Dawson, V. L., Dawson, T.M., Stevens, B., Barres, B.A., 2017. Neurotoxic reactive astrocytes are induced by activated microglia. Nature 541, 481–487.

Livak, K.J., Schmittgen, T.D., 2001. Analysis of relative gene expression data using real-time quantitative PCR and the 2(-Delta Delta C(T)) method. Methods 25, 402–408.

Ludwin, S.K., Rao, Vts, Moore, C.S., Antel, J.P., 2016. Astrocytes in multiple sclerosis. Mult. Scler. 22, 1114–1124.

Lui, H., Zhang, J., Makinson, S.R., Cahill, M.K., Kelley, K.W., Huang, H.Y., Shang, Y., Oldham, M.C., Martens, L.H., Gao, F., Coppola, G., Sloan, S.A., Hsieh, C.L., Kim, C.C., Bigio, E.H., Weintraub, S., Mesulam, M.M., Rademakers, R., Mackenzie, I.R., Seeley, W.W., Karydas, A., Miller, B.L., Borroni, B., Ghidoni, R., Farese Jr., R.V., Paz, J.T., Barres, B.A., Huang, E.J., 2016. Progranulin deficiency promotes circuit-specific synaptic pruning by microglia via complement activation. Cell 165, 921–935.

Mandolesi, G., Gentile, A., Musella, A., Fresegna, D., De Vito, F., Bullitta, S., Sepman, H., Marfia, G.A., Centonze, D., 2015. Synaptopathy connects inflammation and neurodegeneration in multiple sclerosis. Nat. Rev. Neurol. 11, 711–724.

Michailidou, I., Willems, J.G., Kooi, E.J., van Eden, C., Gold, S.M., Geurts, J.J., Baas, F., Huitinga, I., Ramaglia, V., 2015. Complement C1q-C3-associated synaptic changes in multiple sclerosis hippocampus. Ann. Neurol. 77, 1007–1026.

Michailidou, I., Naessens, D.M., Hametner, S., Guldenaar, W., Kooi, E.J., Geurts, J.J., Baas, F., Lassmann, H., Ramaglia, V., 2017. Complement C3 on microglial clusters in

multiple sclerosis occur in chronic but not acute disease: implication for disease pathogenesis. Glia 65, 264–277.

Mishra, D., Richard, J.E., Maric, I., Porteiro, B., Haring, M., Kooijman, S., Musovic, S., Eerola, K., Lopez-Ferreras, L., Peris, E., Grycel, K., Shevchouk, O.T., Micallef, P., Olofsson, C.S., Wernstedt Asterholm, I., Grill, H.J., Nogueiras, R., Skibicka, K.P., 2019. Parabrachial interleukin-6 reduces body weight and food intake and increases thermogenesis to regulate energy metabolism. Cell Rep. 26 (3011–26), e5.

Morrow, S.A., Drake, A., Zivadinov, R., Munschauer, F., Weinstock-Guttman, B., Benedict, R.H., 2010. Predicting loss of employment over three years in multiple sclerosis: clinically meaningful cognitive decline. Clin. Neuropsychol. 24, 1131–1145.

Nataf, S., Carroll, S.L., Wetsel, R.A., Szalai, A.J., Barnum, S.R., 2000. Attenuation of experimental autoimmune demyelination in complement-deficient mice. J. Immunol. 165, 5867–5873.

Pekna, M., Hietala, M.A., Rosklint, T., Betsholtz, C., Pekny, M., 1998. Targeted disruption of the murine gene coding for the third complement component (C3). Scand. J. Immunol. 47, 25–29.

Planche, V., Panatier, A., Hiba, B., Ducourneau, E.G., Raffard, G., Dubourdieu, N., Maitre, M., Leste-Lasserre, T., Brochet, B., Dousset, V., Desmedt, A., Oliet, S.H., Tourdias, T., 2017a. Selective dentate gyrus disruption causes memory impairment at the early stage of experimental multiple sclerosis. Brain Behav. Immun. 60, 240–254.

Planche, V., Ruet, A., Charre-Morin, J., Deloire, M., Brochet, B., Tourdias, T., 2017b. Pattern separation performance is decreased in patients with early multiple sclerosis. Brain Behav. 7, e00739.

Planche, V., Ruet, A., Coupe, P., Lamargue-Hamel, D., Deloire, M., Pereira, B., Manjon, J. V., Munsch, F., Moscufo, N., Meier, D.S., Guttmann, C.R., Dousset, V., Brochet, B., Tourdias, T., 2017c. Hippocampal microstructural damage correlates with memory impairment in clinically isolated syndrome suggestive of multiple sclerosis. Mult. Scler. 23, 1214–1224.

Planche, V., Koubiyr, I., Romero, J.E., Manjon, J.V., Coupe, P., Deloire, M., Dousset, V., Brochet, B., Ruet, A., Tourdias, T., 2018. Regional hippocampal vulnerability in early multiple sclerosis: dynamic pathological spreading from dentate gyrus to CA1. Hum. Brain Mapp. 39, 1814–1824.

Ricklin, D., Lambris, J.D., 2013. Complement in immune and inflammatory disorders: pathophysiological mechanisms. J. Immunol. 190, 3831–3838.

Rocca, M.A., Barkhof, F., De Luca, J., Frisen, J., Geurts, J.J.G., Hulst, H.E., Sastre-Garriga, J., Filippi, M., Magnims Study Group, 2018. The hippocampus in multiple sclerosis. Lancet Neurol. 17, 918–926.

Sahu, A., Rawal, N., Pangburn, M.K., 1999. Inhibition of complement by covalent attachment of rosmarinic acid to activated C3b. Biochem. Pharmacol. 57, 1439–1446.

Schafer, D.P., Lehrman, E.K., Kautzman, A.G., Koyama, R., Mardinly, A.R., Yamasaki, R., Ransohoff, R.M., Greenberg, M.E., Barres, B.A., Stevens, B., 2012. Microglia sculpt postnatal neural circuits in an activity and complement-dependent manner. Neuron 74, 691–705.

Shi, Q., Colodner, K.J., Matousek, S.B., Merry, K., Hong, S., Kenison, J.E., Frost, J.L., Le, K.X., Li, S., Dodart, J.C., Caldarone, B.J., Stevens, B., Lemere, C.A., 2015.

Complement C3-deficient mice fail to display age-related hippocampal decline. J. Neurosci. 35, 13029–13042.

Shi, Q., Chowdhury, S., Ma, R., Le, K.X., Hong, S., Caldarone, B.J., Stevens, B., Lemere, C. A., 2017. Complement C3 deficiency protects against neurodegeneration in aged plaque-rich APP/PS1 mice. Sci. Transl. Med. 9.

Sicotte, N.L., Kern, K.C., Giesser, B.S., Arshanapalli, A., Schultz, A., Montag, M., Wang, H., Bookheimer, S.Y., 2008. Regional hippocampal atrophy in multiple sclerosis. Brain 131, 1134–1141.

Sierra, A., Tremblay, M.E., Wake, H., 2014. Never-resting microglia: physiological roles in the healthy brain and pathological implications. Front. Cell. Neurosci. 8, 240.

Small, S.A., 2014. Isolating pathogenic mechanisms embedded within the hippocampal circuit through regional vulnerability. Neuron 84, 32–39.

Stephan, A.H., Barres, B.A., Stevens, B., 2012. The complement system: an unexpected role in synaptic pruning during development and disease. Annu. Rev. Neurosci. 35, 369–389.

Stevens, B., Allen, N.J., Vazquez, L.E., Howell, G.R., Christopherson, K.S., Nouri, N., Micheva, K.D., Mehalow, A.K., Huberman, A.D., Stafford, B., Sher, A., Litke, A.M., Lambris, J.D., Smith, S.J., John, S.W., Barres, B.A., 2007. The classical complement cascade mediates CNS synapse elimination. Cell 131, 1164–1178.

Szalai, A.J., Hu, X., Adams, J.E., Barnum, S.R., 2007. Complement in experimental autoimmune encephalomyelitis revisited: C3 is required for development of maximal disease. Mol. Immunol. 44, 3132–3136.

t Hart, B.A., Gran, B., Weissert, R., 2011. EAE: imperfect but useful models of multiple sclerosis. Trends Mol. Med. 17, 119–125.

Veerhuis, R., Nielsen, H.M., Tenner, A.J., 2011. Complement in the brain. Mol. Immunol. 48, 1592–1603.

Watkins, L.M., Neal, J.W., Loveless, S., Michailidou, I., Ramaglia, V., Rees, M.I., Reynolds, R., Robertson, N.P., Morgan, B.P., Howell, O.W., 2016. Complement is activated in progressive multiple sclerosis cortical grey matter lesions. J. Neuroinflammation 13, 161.

Werneburg, S., Jung, J., Kunjamma, R.B., Ha, S.K., Luciano, N.J., Willis, C.M., Gao, G., Biscola, N.P., Havton, L.A., Crocker, S.J., Popko, B., Reich, D.S., Schafer, D.P., 2020. Targeted complement inhibition at synapses prevents microglial synaptic engulfment and synapse loss in demyelinating disease. Immunity 52 (167–82), e7.

Wu, T., Dejanovic, B., Gandham, V.D., Gogineni, A., Edmonds, R., Schauer, S., Srinivasan, K., Huntley, M.A., Wang, Y., Wang, T.M., Hedehus, M., Barck, K.H., Stark, M., Ngu, H., Foreman, O., Meilandt, W.J., Elstrott, J., Chang, M.C., Hansen, D. V., Carano, R.A.D., Sheng, M., Hanson, J.E., 2019. Complement C3 is activated in human AD brain and is required for neurodegeneration in mouse models of amyloidosis and Tauopathy. Cell Rep. 28 (2111–23), e6.

Ziehn, M.O., Avedisian, A.A., Tiwari-Woodruff, S., Voskuhl, R.R., 2010. Hippocampal CA1 atrophy and synaptic loss during experimental autoimmune encephalomyelitis, EAE. Lab. Investig. 90, 774–786.

Ziehn, M.O., Avedisian, A.A., Dervin, S.M., Umeda, E.A., O'Dell, T.J., Voskuhl, R.R., 2012. Therapeutic testosterone administration preserves excitatory synaptic transmission in the hippocampus during autoimmune demyelinating disease. J. Neurosci. 32, 12312–12324.